A&A 563, A120 (2014)
DOI: 10.1051/0004-6361/201323230

Astronomy & Astrophysics

Revised physical elements of the astrophysically important O9.5+O9.5V eclipsing binary system Y Cygni⋆,⋆⋆,⋆⋆⋆

P. Harmanec[1], D. E. Holmgren[2], M. Wolf[1], H. Božić[3], E. F. Guinan[4], Y. W. Kang[5], P. Mayer[1], G. P. McCook[4], J. Nemravová[1], S. Yang[6], M. Šlechta[7], D. Ruždjak[3], D. Sudar[3], and P. Svoboda[8]

[1] Astronomical Institute of the Charles University, Faculty of Mathematics and Physics, V Holešovičkách 2, 180 00 Praha 8 – Troja, Czech Republic
e-mail: Petr.Harmanec@mff.cuni.cz
[2] SMART Technologies, 3636 Research Road N.W., Calgary, Alberta, T2L 1Y1 Canada
[3] Hvar Observatory, Faculty of Geodesy, Zagreb University, Kačiéva 26, 10000 Zagreb, Croatia
[4] Department of Astronomy and Astrophysics, Villanova University, Villanova, PA 19085, USA
[5] Dept. of Earth Sciences, Sejong University Seoul, 143-747 Seoul, Korea
[6] Physics & Astronomy Department, University of Victoria, PO Box 3055 STN CSC, Victoria, BC, V8W 3P6, Canada
[7] Astronomical Institute, Academy of Sciences of the Czech Republic, 251 65 Ondřejov, Czech Republic
[8] TRIBASE Net, ltd., Výpustky 5, 614 00 Brno, Czech Republic

Received 11 December 2013 / Accepted 23 January 2014

ABSTRACT

Context. Rapid advancements in light-curve and radial-velocity curve modelling, as well as improvements in the accuracy of observations, allow more stringent tests of the theory of stellar evolution. Binaries with rapid apsidal advance are particularly useful in this respect since the internal structure of the stars can also be tested.
Aims. Thanks to its long and rich observational history and rapid apsidal motion, the massive eclipsing binary Y Cyg represents one of the cornerstones of critical tests of stellar evolutionary theory for massive stars. Nevertheless, the determination of the basic physical properties is less accurate than it could be given the existing number of spectral and photometric observations. Our goal is to analyse all these data simultaneously with the new dedicated series of our own spectral and photometric observations from observatories widely separated in longitude.
Methods. We obtained new series of *UBV* observations at three observatories separated in local time to obtain complete light curves of Y Cyg for its orbital period close to 3 days. This new photometry was reduced and carefully transformed to the standard *UBV* system using the HEC22 program. We also obtained new series of red spectra secured at two observatories and re-analysed earlier obtained blue electronic spectra. Reduction of the new spectra was carried out in the IRAF and SPEFO programs. Orbital elements were derived independently with the FOTEL and PHOEBE programs and via disentangling with the program KOREL. The final combined solution was obtained with the program PHOEBE.
Results. Our analyses provide the most accurate value of the apsidal period of (47.805 ± 0.030) yr published so far and the following physical elements: $M_1 = 17.72 \pm 0.35\ M_\odot$, $M_2 = 17.73 \pm 0.30\ M_\odot$, $R_1 = 5.785 \pm 0.091\ R_\odot$, and $R_2 = 5.816 \pm 0.063\ R_\odot$. The disentangling thus resulted in the masses, which are somewhat higher than all previous determinations and virtually the same for both stars, while the light curve implies a slighly higher radius and luminosity for star 2. The above empirical values imply the logarithm of the internal structure constant $\log\ k_2 = -1.937$. A comparison with Claret's stellar interior models implies an age close to 2×10^6 yr for both stars.
Conclusions. The claimed accuracy of modern element determination of 1–2 per cent still seems a bit too optimistic and obtaining new high-dispersion and high-resolution spectra is desirable.

Key words. binaries: spectroscopic – stars: fundamental parameters – stars: individual: Y Cyg – binaries: close

1. Introduction

The initial motivation of this study was to search for possible line-profile variability in early-type binary systems, and to derive new orbital and physical properties of stars in eclipsing binaries. This project (known as SEFONO) has been discussed in detail in the first two papers of this series devoted to V436 Per and β Sco (see Harmanec et al. 1997; and Holmgren et al. 1997). This paper is devoted to a detailed study of the astrophysically important high-mass eclipsing system Y Cyg. While compiling and analyzing the rich series of its observations, we realised that for such a well-studied system it is valuable to investigate how sensitive the determination of its basic physical properties is to the various assumptions about the input physics and also to the methods of analysis used.

Y Cygni (HD 198846, BD+34°4184) is a very interesting system from the point of view of the theory of stellar structure. It is a double-lined spectroscopic and eclipsing binary with an eccentric orbit of 2.996 d and a relatively rapid apsidal motion ($P_{\rm aps.} = 48$ yr). Y Cyg was among the very first binaries for

⋆ Based on new spectral and photometric observations from the following observatories: Dominion Astrophysical Observatory, Hvar, Ondřejov, Fairborn, and Sejong.
⋆⋆ Appendix A is available in electronic form at http://www.aanda.org
⋆⋆⋆ Tables 4 and 5 are available at the CDS via anonymous ftp to cdsarc.u-strasbg.fr (130.79.128.5) or via http://cdsarc.u-strasbg.fr/viz-bin/qcat?J/A+A/563/A120

which the apsidal motion was convincingly detected. Thanks to this, it became the subject of numerous studies. The history of its investigation is summarised in the papers by Hill & Holmgren (1995) and Holmgren et al. (1995) and need not be repeated here. We only mention some more recent studies relevant to the topic. Simon & Sturm (1992, 1994) developed a new technique of spectra disentangling, which permits the separation of the spectra of binary components with a simultaneous determination of the orbital and physical elements. Simon et al. (1994) applied this technique to a study of Y Cyg. Comparing the disentangled and synthetic spectra, they obtained a new estimate of the $T_{\rm eff}$ and log g for both components. New orbital elements of Y Cyg were derived from the published radial velocities (RVs) of Hill & Holmgren (1995) by Karami & Teimoorinia (2007), who used a least-squares technique, and by Karami et al. (2009), who used the artificial neural network method and who arrived at virtually identical masses for both stars.

Several authors argued in favour of the presence of stellar wind in Y Cyg. Morrison & Garmany (1984) studied and modelled the resonance C IV and N V UV lines in the spectra from the International Ultraviolet Explorer (IUE). They found the lines are blue-shifted for some 160 km s^{-1} with respect to photospheric lines, derived a terminal velocity of 1500 km s^{-1}, and estimated a rather moderate mass-loss rate of $10^{-8.4}$ $M_\odot$ yr^{-1}. Koch & Pfeiffer (1989) studied polarimetric changes of Y Cyg and concluded that there is some evidence of hot material between the stars, although they admitted that the observed variations are not large, and argued again in favour of the presence of stellar wind. Their B-band polarimetric observations were later reanalyzed by Fox (1994), who could not find any periodicity related to the binary orbit. He noted that there was some evidence from observations close to binary eclipses that one of the stars possesses a stellar wind. Finally, Pfeiffer et al. (1994) studied and modelled the stellar wind from the UV line profiles of C IV and Si IV. To this we should add that our Hα spectra do not show any detectable emission.

In spite of all the efforts, the basic physical properties of the system have not been derived accurately enough. This is mainly because of the awkward orbital period that is very close to 3 days. Another complication is a close similarity of the spectra of both stars and a mass ratio near 1.0. In Table 1 we summarize the values of the mass ratio and individual masses derived by various investigators. Since different investigators of Y Cyg have identified the primary and secondary differently, we shall not use the terms *primary* and *secondary*, but will call the components *star 1* and *star 2*, with the convention that the minimum RV of star 1 occurs near JD 2 446 308.97 for the sidereal orbital period of 2.99633179 d (see below).

Usually, the apsidal motion was investigated on the basis of existing times of photometric minima. In spite of the obvious importance of this binary, no really complete light curve has been obtained within one specific epoch, and a light curve in a standard system has not been obtained yet. This has prevented the determination of the individual colours of the binary components, and therefore their temperatures.

There are several motivations for this study.

1. Hill & Holmgren (1995) write in their section on photometry: "We do not consider this photometric solution to be definitive and hope that Y Cyg will be observed again over a 4 year span in a fully calibrated system." We circumvent this requirement by combining our efforts from three stations, suitably separated in local time. In 1999, we obtained calibrated UBV photometry of the binary from North America, Europe, and Korea. Additionally, we also have new Reticon and CCD spectra of Y Cyg at our disposal.
2. For such an astrophysically important system, it was deemed useful to explore the effect of different physical assumptions and different methods of analyses on the result and to see what accuracy in the determination of the basic physical properties can actually be achieved.
3. We profit from having at our disposal the reduction procedures that allow separate or simultaneous RV and light-curve solutions, with the rate of apsidal advance as one of the elements of the solution. This gives us the chance to use all available, as well as our new observations in the determination of all basic physical elements of the binary with an unprecedented accuracy and to define a more or less definitive orbit.
4. Thanks to the disentangling technique, we are also able to test for the presence of rapid line-profile changes, which could be related to forced non-radial oscillations.

Here, we report our results.

Table 1. Individual masses and the mass ratio M_2/M_1 derived by various investigators.

M_2/M_1	$M_1 \sin^3 i$ ($M_\odot$)	$M_2 \sin^3 i$ ($M_\odot$)	Source	Note
0.922	16.5	15.2	A	
1.011	17.2	17.4	B	
1.037	16.4 ± 0.3	17.0 ± 0.3	C	
1.024	16.6 ± 0.2	17.0 ± 0.3	D	
1.031	16.94 ± 0.11	17.47 ± 0.11	E	*
0.949	17.6 ± 0.4	16.7 ± 0.5	F	*
0.989	17.4 ± 0.3	17.2 ± 0.2	G	
1.002	17.1 ± 0.4	17.14 ± 0.12	H	
0.998	17.26 ± 0.22	17.22 ± 0.22	I	

Notes. Since different authors alternatively denoted one or the other component of the pair as the primary, we adopt the convention that star 1 is the component that has the minimum RV near JD 2 446 308.97 for the sidereal orbital period of 2.99633179 d (see the text below). Abbreviations used in Col. 4: A) Plaskett (1920); B) Redman (1930); C) Vitrichenko (1971); D) Stickland et al. (1992); E) Simon et al. (1994); F) Burkholder et al. (1997); G) Hill & Holmgren (1995); H) Karami & Teimoorinia (2007); I) Karami et al. (2009). An asterisk in Col. 5 denotes that the role of the components is inverted with respect to our convention in the original study.

2. Observations and reductions

2.1. Spectroscopy

Spectroscopic observations at our disposal consist primarily of the following three series of electronic spectrograms obtained at Dominion Astrophysical Observatory (DAO):

- 43 Reticon blue spectra already used by Hill & Holmgren (1995);
- 9 Reticon blue spectra obtained with the 1.83 m reflector and 21121 spectrograph configurations by DH;
- 19 red CCD spectra secured by SY with the 1.2 m reflector.

For further details on the DAO 21121, 21181 and 9681 spectrographs, we refer the reader to Richardson (1968).

Additionally, we also used two CCD spectra secured by MW at the coudé focus of the Ondřejov 2 m reflector.

Table 2. RV data sets.

Spectrograph No.	Epoch (RJD = HJD-2 400 000)	No. of RVs prim/s	Dispersion (Å mm^{-1})	Wavelength range (Å)	Source
1	22 177.8–22 546.8	21/22	29, 49	3900–5000	A
1	22 570.9–25 841.0	45/50	29, 49, 90	3900–5000	B
1	27 284.8–28 026.8	35/35	14.8, 21.5, 29, 49		D
2	34 527.8–36 028.0	27/27	36, 40	3800–4700	C
3	36 028.9–36 360.9	17/17	10	3800–6700	C
1	36 050.9–39 116.6	37/37	14.8, 29, 49		D
4	39 404.3–39 991.4	26/26	37		E
5	44 121.6–48 042.8	42/42	0.9–1.4	1500–	F
6	48 105.4–49 203.5	42/42	9.9	4000–4680	G
7	48 142.8–48 951.7	29/29	~10	4010–4970	H
8	45 897.8–45 909.8	14/08	20	3961–4510	I
8	46 305.0–48 545.8	29/28	20	3970–4510	I
9	46 694.8–47 017.9	09/09	15	3760–4195	J
10	51 393.9–55 220.6	25/25	10	6150–6755	J
11	54 027.3–54 084.2	02/02	17.2	6255–6767	J

Notes. Column 1: 1) Dominion Astrophysical Observatory 1.83 m reflector, 1-prism and 2-prism spg., IL, IM, IS, ISS and IIM configurations; 2) MtWilson 60-inch, γ and X prism spgs.; 3) MtWilson 100-inch coudé grating spg.; 4) Crimea 1.22 m reflector; 5) International Ultraviolet Explorer, SPW high-dispersion spectra; 6) Calar Alto 2.2 m reflector, coudé spg., TEK CCD; 7) Kitt Peak Coudé Feed spg.; 8) Dominion Astrophysical Observatory 1.22 m reflector, coudé grating spg., Reticon 1872RF; 9) Dominion Astrophysical Observatory 1.83 m reflector, Cassegrain grating spg., Reticon 1872RF; 10) Dominion Astrophysical Observatory 1.22 m reflector, coudé grating spg., CCD SiTE-4 detector; 11) Ondřejov Observatory 2.0 m reflector, coudé spg., CCD SiTE-5. Abbreviations used in Col. 6: A) Plaskett (1920), remeasured by Redman (1930); B) Redman (1930); C) Struve et al. (1959), partly remeasured by Huffer & Karle (1959); D) this paper; unpublished RV measurements by Pearce and Petrie; E) Vitrichenko (1971); F) Stickland et al. (1992); G) Simon & Sturm (1994); H) Burkholder et al. (1997); I) Hill & Holmgren (1995) and this paper; J) this paper.

In all cases, calibration arc frames were obtained before and after each stellar frame. During each night, series of ten flat–field and ten bias exposures were obtained at the beginning, middle, and end of the night. These were later averaged for the processing of the stellar data frames. For the 1.83 m data, exposure times ranged from 15 to 30 min, with the signal-to-noise ratio (S/N) between 70 and 150, while for the 1.2 m data exposure times of 20 min were used, giving S/N between 32 and 180. The data obtained by DH were re-reduced by SY with IRAF, from initial extraction and flat-fielding up to wavelength calibration. The Ondřejov spectra were also reduced this way by MŠ in IRAF. Continuum rectification of all spectra and cleaning from cosmic ray hits (cosmics) was carried out by PH using the program SPEFO (see Horn et al. 1996; Škoda 1996). Following Horn et al. (1996), we also measured a selection of good telluric lines in all red spectra and used the difference between the calculated heliocentric RV correction and the mean RV of these telluric lines to bring all red spectra into one RV zero point.

To be able to derive the new, most accurate value of the rate of apsidal advance, we also compiled all available RVs from the astronomical literature, which can be found in Table 2. Here, and in several other tables we give the time instants in an abbreviated form: RJD = HJD – 2 400 000.0. We could not use three 1913–1914 Mt Wilson RVs published by Abt (1973) since they obviously refer to unresolved lines of both stars. A few comments are appropriate. For the older DAO data, we adopted the re-measurement by Redman (1930). For those McDonald RVs that were measured more than once, we calculated and adopted mean RVs for each multiple measurement. The only exception was the spectrum taken on Jul 7, 1957 at 10:31 UT for which Huffer & Karle (1959) measured very deviating values. We adopted the original RVs from Struve et al. (1959) for this particular spectrogram. We also omitted the McDonald spectrum obtained on May 1, 1957 (HJD 2 436 324.9349), for which Struve et al. (1959) tabulate a very deviant value, the same for both components (as also seen in their original phase diagram). For the new spectra at our disposal, the RVs were derived via Gaussian fits to the line profiles of He I 4026 Å (blue spectra) and He I 6678 Å (red spectra). Finally, for the electronic spectra at our disposal, we also derived new orbital solutions using the KOREL disentangling technique by Hadrava (1995, 1997, 2004b, 2005) for several stronger lines (as discussed in detail below).

2.2. Photometry

Several photoelectric light curves of Y Cyg have been published. The star has also been observed by HIPPARCOS and new *UBV* observations were secured during the 1999 observing campaign in Hvar, Korea, and with the Four College APT in Arizona. Hvar observations continued in 2006–2007 and 2009. In 2006, two eclipses in *BVR* were observed by PS. Basic information on all available data sets can be found in Table 3 and illustrative light curves based on our new observations are shown in Fig. 1.

It was very unfortunate that different observers used different comparison stars, even the red ones. However, most of the data sets were obtained relative to HD 199007.

An important part of our new observations was, therefore, to observe all these comparisons and to derive their good all-sky *UBV* magnitudes. Adding these to the magnitude differences variable minus comparison allowed us to get many of the published data sets closer to the standard *UBV* system. More details on the data reduction and homogenization can be found in the Appendix.

To derive new, improved values of the orbital and apsidal period, we also used the historical light curve by Dugan (1931), adopting $V = 9^{\rm m}.402$ (based on the Hvar observations) for his comparison star SAO 70600 = BD+33°4062.

Table 3. Photoelectric observations of Y Cyg.

Source	Station No.	Epoch (RJD)	No. of obs. *U*/*B*/*V*	No. of nights	$HD_{comp.}$/ HD_{check}	Passbands used
1	74	33 827.3–36 071.4	347	49	198820/197419	no filter ef. 4200 Å
2	76	36 808.4–37 589.4	155/29	7/2	198692/199007	filters 4550 and 6000 Å
3	71	39 712.3–40 528.4	21/104/104	10	199007/ –	*UBV*
3	19	41 119.4–41 154.5	48	5	199007/ –	*UBV*
3	42	41 145.8–41 190.8	7	3	199007/ –	*UBV*
3	75	41 159.4–41 193.5	24/23	8	199007/ –	*BV*
3	72	41 169.7–42 577.9	90/87/103	4/4/5	199007/ –	*UBV*
4	70	44 081.4–44 083.7	127	2	199007/ –	*B*
7	94	47 769.4–47 788.5	60	6	199007/ –	*V*
5	61	47 890.4–49 040.7	141	36	all-sky	*V*
6	77	48 040.1–48 042.8	33	3	all-sky	*V* (IUE FES sensor)
7	54	48 178.3–48 182.3	140	5	199007/ –	*V*
8	01	51 371.6–51 377.4	10	4	204403/202349	*UBV*
8	01	51 379.4–51 448.3	141	13	202349/204403	*UBV*
8	01	54 011.3–54 020.5	93	5	202349/199007, 198820	*UBV*
8	01	55 113.3–55 126.4	65	13	199007/198692, 198820	*UBV*
8	16	51 452.6–51 457.8	79	6	204403/199007	*UBV*
8	16	53 628.6–53 667.8	54	12	204403/199007	*UBV*
8	16	54 008.8–54 070.6	85	10	204403/199007	*UBV*
8	16	54 270.8–54 285.9	79	22	204403/199007	*UBV*
8	78	51 477.0–51 539.0	111	4	199007/204403	*UBV*
8	02	54 025.2–54 405.3	258	3	199007/–	*BVR*

Notes. Abbreviations used in Col. 1: 1) Magalashvili & Kumsishvili (1959); 2) Herczeg (1972); 3) O'Connell (1977); 4) Giménez & Costa (1980); 5) Perryman & ESA (1997); 6) Stickland et al. (1992); 7) Mossakovskaya (2003); 8) this paper. Abbreviations used in Col. 2 (numbers are running numbers of the observing stations from the Praha/Hvar data archives): 01) Hvar 0.65 m reflector, photoelectric photometer; 02) Brno private observatory of P. Svoboda, Sonnar 0.135 m photographic lens and a CCD SBIG 7 camera; 16) Four College 0.80 m APT; 19) Abastumani 0.48 m; 42) Dyer Observatory 0.61 m Seyfert reflector, 1P21 tube; 54) Crimean 0.60 m reflector, EMI 9789 tube; 61) HIPPARCOS H_p magnitude transformed to Johnson *V* after Harmanec (1998); 70) Mojon de Trigo 0.32 m Cassegrain, EMI 6256 A tube; 71) Vatican 0.60 m Cassegrain, 1P21 tube; 72) Dominion Astrophysical Observatory 0.30 m, EMI 6256SA tube; 74) Abastumani 0.33 m; 75) Tübingen 0.40 m reflector; 76) Hoher List 0.35 m reflector; 77) International Ultraviolet Explorer: the fine error sensor 78) Sejong 0.40 m reflector; 94) Kazan station of the SAO 0.48 m reflector.

We provide all individual, homogenised photometric observations together with their heliocentric Julian dates in Table 4.

2.3. Times of minima

We have collected all accurate times of primary and secondary mid-eclipses available in the literature and complemented them with the minima derived on the basis of our photometry. All photoelectric times of minima presented in Holmgren et al. (1995; their Table I) were included. Over 500 reliable times of the primary and secondary minima were used in our analysis. They now span an interval of about 125 years and are all listed in Table 5.

3. Towards a new accurate ephemeris

To derive a new ephemeris including the rate of the apsidal advance, we decided to derive and compare the results of three independent determinations, based on (i) light-curve solutions; (ii) orbital solutions; and (iii) analyses of the times of minima.

To this end, we used two different computer programs, which are widely used and allow the calculation of the light-curve and orbital solutions: the program `FOTEL`, developed by Hadrava (1990, 2004a), and the program `PHOEBE` (Prša & Zwitter 2005, 2006) based on the WD 2004 code (Wilson & Devinney 1971).

We note that `FOTEL` models the shape of the stars as triaxial ellipsoids and uses linear limb-darkening coefficients while `PHOEBE` models the binary components as equipotential surfaces of the Roche model and allows the use of non-linear limb darkening laws. Both programs are, however, particularly well suited for our task since they allow us to derive the rate of the periastron advance as one of the elements.

We first carried out some exploratory solutions to map out the existing uncertainties in the value of the orbital period and the rate of the periastron advance as well as the sensitivity to different limb-darkening coefficients found in the literature. To this end, we first derived various trial solutions independently for the photometric and RV data.

We used all photoelectric *UBV* observations in combination with Dugan's photometry. Altogether, this data set contains 4888 individual data points spanning an interval from HJD 2 420 777.6 to 2 454 405.3 i.e. over 92 years.

3.1. FOTEL exploratory light-curve solutions

The values of the linear limb-darkening coefficients given in various more recent studies are summarized in Table 6. We estimated the values quoted from the paper by Diaz-Cordoves et al. (1995) via interpolation in their Table 1 after finding that their interpolation formula does not perform particularly well near $T_{\rm eff}$ = 30 000 K. To get some idea about how serious the uncertainties in the values of the limb-darkening coefficients are, we derived four exploratory solutions F1 to F4, using subsequently the linear limb-darkening coefficients from the four sources given in Table 6.

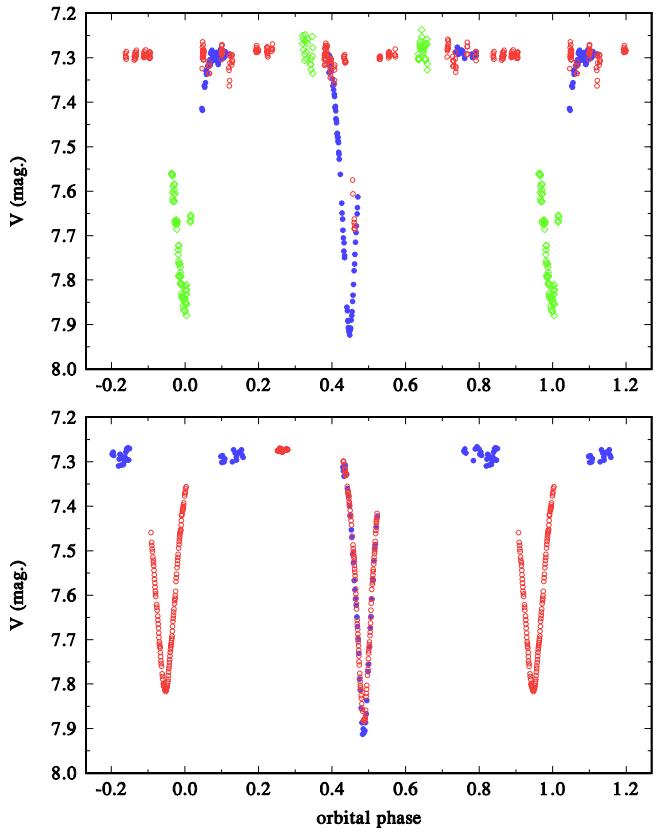

Fig. 1. *V*-band light curves: *Upper panel* shows the 1999 campaign observations. Filled circles/blue in the electronic version denote the Hvar, open circles/red the Villanova APT, and diamonds/green the Sejong individual observations. The *bottom panel* shows the Hvar (filled circles/blue) and Brno (open circles/red) 2006 and 2007 observations. The data are plotted vs. phase of the *sidereal* orbital period, with phase zero corresponding to one instant of the primary mid-eclipse: HJD 2 446 308.3966.

In every case, we first derived a preliminary solution keeping the weights of all data subsets equal to one. Then we weighted individual data sets by the weights inversely proportional to the square of the rms error per one observation from that solution and used them to obtain the final solution. In practice, the weights ranged from 0.27 for Dugan's observations to 20.6 for the best photoelectric observations. All these exploratory solutions are summarized in Table 7. Fortunately, it turned out that the difference between them was much smaller than the respective rms errors of all elements derived.

3.2. PHOEBE exploratory light-curve solutions

For comparison, we also derived a joint exploratory solution, based on all available light curves, using a recent *devel* version of the program PHOEBE (Prša & Zwitter 2005, 2006) and also using linear limb-darkening coefficients from Claret (2000). This solution is denoted P1 in Table 7 and should correspond to solution F4 of that Table. Since PHOEBE also allows the use of several non-linear laws of limb darkening, we also compare (in Table 8) the PHOEBE solution for square-root limb-darkening coefficients adopted from Claret (2000) (solution P2) and square-root law from limb darkening tables, derived by Dr. A. Prša from the new Castelli & Kurucz (2004) model atmospheres. In this last case, the coefficients were interpolated after each iteration for the current effective temperature (solution P3).

Table 6. Linear limb-darkening coefficients in the *UBV* passbands for stars with $T_{\rm eff}$ near 30 000 K and log g of 4.1 to 4.2 given by various authors

Source	*V*	*B*	*U*
Al-Naimiy (1978)	0.27	0.32	0.32
Wade & Rucinski (1985)	0.23	0.29	0.29
Diaz-Cordoves et al. (1995)	0.29	0.34	0.34
Claret (2000)	0.33	0.37	0.38

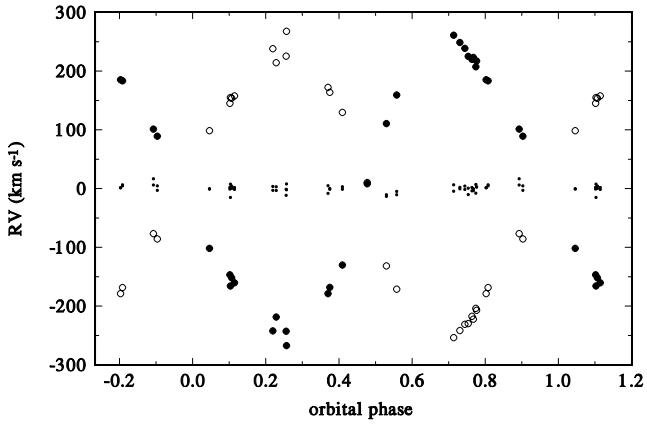

Fig. 2. RV curve based on the RVs from Gaussian fits to the He I 6678 Å line from our new electronic spectra. The data are plotted vs. phase of the *sidereal* orbital period, with phase zero corresponding to the primary mid-eclipse. The small dots denote the residua from the orbital solution.

3.3. FOTEL exploratory orbital solutions

We first derived the orbital elements from all available RVs assigning weight one to all of them. This initial solution is denoted "unweighted" in Table 9. Then we assigned weights inversely proportional to the rms error per one observation from this solution to all ten subsets from different spectrographs and repeated the solution. This improved solution is denoted "weighted" in Table 9. A few things are worth noting. It turned out that the RV measurements based on the Gaussian fits are by far the most accurate of all classical RV measurements. We also note a rather large scatter in the value of the systemic velocity from different instruments. We do not think this is indicative of a real change. It is more likely that this arises from different investigators using different lines (and perhaps different laboratory wavelengths). For O-type stars, the line blending due to line broadening can be quite severe. For instance, the He I 4026 Å line is partly blended with a He II line, which probably explains the most negative systemic velocity for spectrograph (spg.) 9. On the other hand, the true systemic velocity is probably close to that of spg. No. 10; the RVs are based on the Gaussian fit to the He I 6678 Å singlet line.

Since this last RV dataset is obviously the most accurate one, we also present (in Table 10) another FOTEL solution based on these RVs only, keeping the orbital period, eccentricity, and the longitude of periastron fixed from the solution P3 of Table 8. A corresponding RV curve is in Fig. 2.

3.4. Apsidal motion from the analysis of the observed times of minima

To compare different approaches, we analyzed all available times of the observed primary and secondary minima.

Table 7. Exploratory FOTEL and PHOEBE light-curve solutions for all 4888 available yellow, blue, and ultraviolet observations with known times of observations.

Element	$F1$	$F2$	$F3$	$F4$	$P1$
P (d)	2.99633161	2.99633161	2.99633162	2.99633162	2.99633179
$P_{\rm anomal.}$ (d)	2.99684586	2.99684586	2.99684587	2.99684585	2.99684593
	±0.00000016	±0.00000016	±0.00000016	±0.00000016	0.00000070
$T_{\rm peri.}$ (RJD)	46308.66353	46308.66357	46308.66348	46308.66343	46308.66168
	±0.00038	±0.00038	±0.00038	±0.00038	±0.00018
$T_{\rm prim.ecl.}$ (RJD)	46308.39641	46308.39641	46308.39638	46308.39638	46308.39581
e	0.14514 ± 0.00020	0.14512 ± 0.00020	0.14510 ± 0.00020	0.14511 ± 0.00020	0.14522 ± 0.00029
ω (°)	132.474 ± 0.050	132.478 ± 0.050	132.467 ± 0.051	132.460 ± 0.051	132.280 ± 0.094
$\dot{\omega}$ (° d^{-1})	0.0206166	0.0206168	0.0206169	0.0206161	0.020626
	±0.0000069	±0.0000069	±0.0000070	±0.0000070	±0.000013
r_1	0.2029 ± 0.0027	0.2033 ± 0.0030	0.2026 ± 0.0024	0.2021 ± 0.0022	0.1954
r_2	0.2040 ± 0.0017	0.2033 ± 0.0019	0.2043 ± 0.0015	0.2049 ± 0.0014	0.2069
i (°)	86.587 ± 0.013	86.693 ± 0.012	86.619 ± 0.013	86.571 ± 0.014	86.415 ± 0.029

Notes. Solutions F1 to F4 are derived with FOTEL for the linear limb-darkening coefficients published by Al-Naimiy (1978), Wade & Rucinski (1985), Diaz-Cordoves et al. (1995), and Claret (2000), respectively (see Table 6). Solution P1 is derived with the program PHOEBE also using a linear law of the limb darkening and adopting Claret (2000) values. To save space, we only tabulate the basic elements of the solutions.

Table 8. Exploratory PHOEBE light-curve solutions for all 4888 available yellow, blue, and ultraviolet observations with known times of observations, using square-root limb darkening coefficients.

Element	P2	P3
P (d)	2.99633179	2.996331786
$P_{\rm anomal.}$ (d)	2.99684596	2.996846065
	±0.00000070	±0.000000698
$T_{\rm peri.}$ (RJD)	46 308.66176	46 308.66177
	±0.00018	±0.00017
$T_{\rm prim.ecl.}$ (RJD)	46 308.39582	46 308.39576
e	0.14521 ± 0.00029	0.14508 ± 0.00029
ω (°)	132.288 ± 0.094	132.291 ± 0.094
$\dot{\omega}$ (° d^{-1})	0.020614	0.020618
	±0.000013	±0.000013
r_1	0.1959	0.1968
r_2	0.2064	0.2056
i (°)	86.449 ± 0.028	86.693 ± 0.012

Notes. These solutions are derived with PHOEBE for the square-root limb-darkening law. For solution P2 the coefficients were adopted from Claret (2000), while solution P3 is derived in such a way that in each iteration the program interpolates in the new limb-darkening tables derived by Dr. A. Prša from the Castelli & Kurucz (2004) model atmospheres. To save space, we only tabulate the basic elements of the solutions.

To derive improved estimates of the periastron passage for a chosen reference epoch $T_{\rm periastr.}$, sidereal period $P_{\rm sider.}$, eccentricity e, longitude of periastron at the reference epoch ω_0, and the rate of apsidal advance $\dot{\omega}$ (expressed in degrees per 1 day), we employed the method described by Giménez & García-Pelayo (1983) and revised by Giménez & Bastero (1995). This is a weighted least-squares iterative procedure, including terms in the eccentricity up to the fifth power. The periastron position ω is defined by the linear equation

$$\omega = \omega_0 + \dot{\omega}\, E, \tag{1}$$

where E is the epoch of each recorded minimum. The relation between the sidereal period $P_{\rm sider.}$ and the anomalistic period $P_{\rm anom.}$ is given by

$$\frac{1}{P_{\rm anomal.}} = \frac{1}{P_{\rm sider.}} - \frac{\dot{\omega}}{360^\circ}, \tag{2}$$

Table 9. Exploratory FOTEL orbital solutions for all RVs found in the astronomical literature and measured via Gaussian fits in our new spectra.

Element	Unweighted	Weighted
$P_{\rm sider.}$ (d)	2.9963331	2.9963329
$P_{\rm anomal.}$ (d)	2.9968425	2.9968458
	±0.0000052	±0.0000038
$T_{\rm peri.}$ (RJD)	46308.620	46308.637
	±0.016	±0.010
$T_{\rm prim.ecl.}$ (RJD)	46308.380	46308.386
e	0.1335 ± 0.0050	0.1404 ± 0.0032
ω (°)	127.4 ± 2.1	129.6 ± 1.3
$\dot{\omega}$ (°d^{-1})	0.02042 ± 0.00022	0.02056 ± 0.00016
K_1	242.6 ± 1.6	242.77 ± 0.99
K_1/K_2	1.0135 ± 0.0093	1.0118 ± 0.0055
γ_1 (km s^{-1})	−53.0 ± 1.8	−53.0 ± 1.8
γ_2 (km s^{-1})	−62.6 ± 4.0	−62.6 ± 4.0
γ_3 (km s^{-1})	−63.4 ± 5.9	−63.4 ± 5.9
γ_4 (km s^{-1})	−58.9 ± 4.2	−58.9 ± 4.3
γ_5 (km s^{-1})	−68.2 ± 2.1	−68.2 ± 2.1
γ_6 (km s^{-1})	−63.2 ± 1.2	−63.1 ± 1.2
γ_7 (km s^{-1})	−63.6 ± 2.1	−63.7 ± 2.1
γ_8 (km s^{-1})	−52.6 ± 2.0	−52.7 ± 2.0
γ_9 (km s^{-1})	−71.0 ± 1.5	−70.9 ± 1.2
γ_{10} (km s^{-1})	−61.05 ± 0.89	−61.03 ± 0.85
rms (km s^{-1})	23.8	14.5

Notes. The numbering of the individual systemic velocities corresponds to that used in Table 2. We note, however, that since the RV zero point of the red spectra was checked via measurements of a selection of telluric lines, the two Ondřejov spectra of spectrograph 11 were also treated as belonging to spectrograph 9.

and the period of apsidal motion U in days by

$$U = \frac{360^\circ}{\dot{\omega}}. \tag{3}$$

The orbital inclination $i = 86\overset{\circ}{.}6$ was adopted on the basis of our trial light-curve solutions. The resulting elements with their errors are summarized in Table 11 and the corresponding O–C diagram is shown in Fig. 3.

More details about the apsidal-motion solution and the comparison of the present result with the previous studies of apsidal

Table 10. Another exploratory FOTEL orbital solution based on the most accurate He I 6678 Å RVs measured via Gaussian fits in our new electronic spectra.

Element	Value
$P_{\rm sider.}$ (d)	2.99633179 fixed
$P_{\rm anomal.}$ (d)	2.99684607 fixed
$T_{\rm peri.}$ (RJD)	46308.6612
	±0.0027
$T_{\rm prim.ecl.}$ (RJD)	46308.3952
e	0.14508 fixed
ω (°)	132.291 fixed
K_1	245.9 ± 1.5
K_1/K_2	1.0210 ± 0.0092
γ_{10} (km s^{-1})	−61.13 ± 0.84
rms (km s^{-1})	6.12

Table 11. Elements derived from the analysis of the observed times of the primary and secondary minima.

Element	Value
$P_{\rm sider.}$ (days)	2.99633210 ± 0.00000031
$P_{\rm anomal.}$ (days)	2.99684726 ± 0.00000031
$T_{\rm prim.ecl.}$ (RJD)	46308.39655 ± 0.00035
e	0.1448 ± 0.0012
ω (degrees)	132.54 ± 0.18
$\dot{\omega}$ (deg. per day)	0.020648 ± 0.00009
U (years)	47.73 ± 0.21

motion by Giménez et al. (1987) and Holmgren et al. (1995) can be found in a recent conference paper by Wolf et al. (2013).

3.5. Adopted ephemeris

Comparing the results obtained in three different ways, which are summarized in Tables 7, 8, 9, and 11, we conclude that PHOEBE solution P3 in Table 8, based on several thousands of individual photometric observations spanning 33 628 days and the most detailed physical assumptions, provides the best current ephemeris for the system. We adopt the period and the rate of the apsidal advance from this solution and we use them consistently in all the following analyses. We note that it implies the period of apsidal motion $U = (47.805 \pm 0.030)$ yr.

3.6. Spectra disentangling for the electronic spectra

As already mentioned, we used the program KOREL developed by Hadrava (1995, 1997, 2004b, 2005) for the spectra disentangling. Preparation of data for the program KOREL deserves a few comments. The electronic spectra at our disposal have different spectral resolutions. The DAO spectra with the dispersion of 20 Å mm^{-1} (spg. 8 in Table 2) are recorded with a wavelength step of 0.3 Å which translates to a RV resolution ranging from 22.7 km s^{-1} at the blue end to 19.9 km s^{-1} at the red red. The 15 Å mm^{-1} DAO spectra (spg. 9 of Table 2) have a 0.235 Å separation between two consecutive pixels which translates to 18.7–16.8 km s^{-1}. The corresponding values for the red DAO and Ondřejov spectra are 0.150 Å, i.e. 7.3–6.5 km s^{-1} and 0.256 Å and 12.3–11.4 km s^{-1}. We note that KOREL and the Fast Fourier Transform (FFT) used in that program require that the input spectra are rebinned into equidistant steps in RV in such a way that the number of data points in each spectrum is an integer power of 2. We also note that the two subsets of the blue DAO Reticon spectra cover two overlapping spectral regions. For this reason, we investigated the following three spectral regions with KOREL, using the RV steps to satisfy the above conditions:

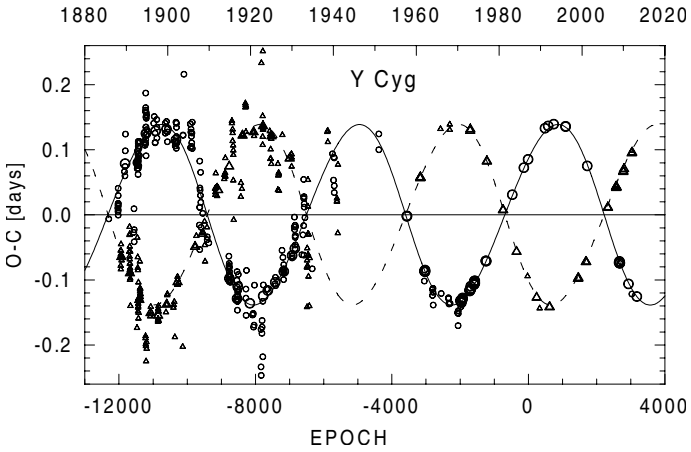

Fig. 3. O–C diagram for the times of minimum of Y Cyg. The continuous and dashed curves represent predictions for the primary and secondary eclipses. The individual primary and secondary minima are shown as circles and triangles. Larger symbols correspond to the photoelectric or CCD measurements which were given higher weights in the calculations.

4003–4180 Å, RV step 14.2 km s^{-1},

4175–4495 Å, RV step 11.5 km s^{-1}, and

6340–6740 Å, RV step 4.75 km s^{-1}.

We omitted the blue DAO spectra r3049 to r4136 (RJDs 46 304.97 to 46 330.78) that were used by Hill & Holmgren (1995), because there was a technical problem with the Reticon detector at that time and the spectra are very poor and strongly underexposed. We also omitted another very poor spectrum r7712 (RJD 46 611.79). The rebinning was carried out with the help of the program HEC35D written by PH[1] which derives consecutive discrete wavelengths via

$$\lambda_n = \lambda_1 \left(1 + \frac{\triangle RV}{c}\right)^{n-1}, \quad (4)$$

where λ_1 is the chosen initial wavelength, $\triangle RV$ is the constant step in RV between consecutive wavelengths, and λ_n is the wavelength of the nth rebinned pixel. Relative fluxes for these new wavelength points are derived using the program INTEP (Hill 1982), which is a modification of the Hermite interpolation formula. It is possible to choose the initial and last wavelength and the program smoothly fills in the rebinned spectra with continuum values of 1.0 at both edges.

To take the variable quality of individual spectra into account, we measured their S/N ratios in the line-free region 4170–4179 Å for the blue spectra, and 6635–6652 Å for the red spectra, and assigned each spectrum a weight according to formula

$$w = \frac{(S/N)^2}{(S/N_{\rm mean})^2}, \quad (5)$$

where $S/N_{\rm mean}$ denotes the mean S/N ratio of all spectra. Specifically, the S/N ranged between 42 and 355 for the blue,

[1] The program HEC35D with User's Manual is available to interested users at ftp://astro.troja.mff.cuni.cz/hec/HEC35

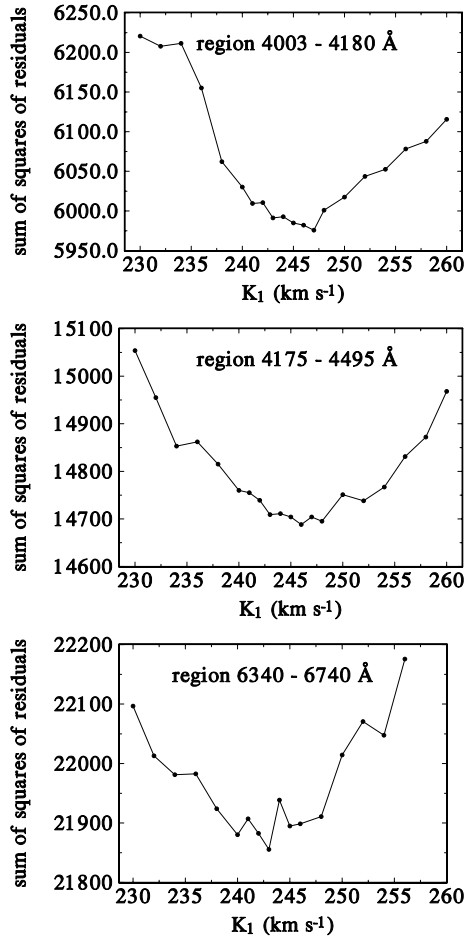

Fig. 4. Search for the best value of the semiamplitude of star 1 with KOREL in three spectral regions, keeping the mass ratio fixed at the value of 1.012.

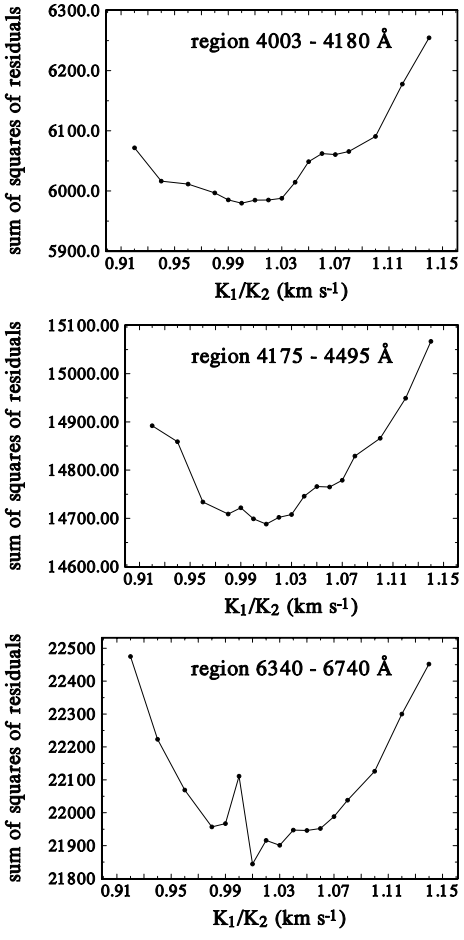

Fig. 5. Search for the best value of the mass ratio K_1/K_2 with KOREL in three spectral regions, keeping the semi-amplitude of the star 1 equal to 243, 245, and 246 km s^{-1}, respectively (resulting from the minima of the K_1 maps).

and between 66 and 262 for the red spectra. We note that KOREL uses the observed spectra and derives both, the orbital elements and the mean individual line profiles of the two binary components.

We first investigated the variation of the sum of squares as a function of the semiaplitude of star 1 and the mass ratio, considering our experience that the sum of squares has a number of local minima. These maps for the semiamplitude K_1 and the mass ratio $q = K_1/K_2$ for all three considered spectral regions are shown in Figs. 4 and 5, respectively. They show that the most probable value of K_1 is around 245 km s^{-1}; for q this is close to 1.01. The final KOREL solutions for the three available wavelength intervals were then derived via free convergency starting with the values close to those corresponding to the lowest sum of squares found from our two-parameter maps. We kicked the parameters somewhat from their optimal values and ran a number of solutions to find the one with the lowest sum of residuals in each spectral region. In the initial attempts, we verified that the values of e and ω from the KOREL solutions agree reasonably with those from the photometric solutions. To decrease the number of free paramaters, we also fixed the value of the orbital eccentricity from the photometric solutions at 0.1451 and ran another series of KOREL solutions to find those with the lowest sum of squares of residuals. These were adopted as final and are summarized in Table 12.

Table 12. KOREL disentangling orbital solutions for three spectral regions.

Element	4003–4180 Å	4175–4495 Å	6340–6740 Å
$T_{\rm periastr.}$	46 308.6618	46 308.6562	46 308.6635
e	0.14448	0.14929	0.14640
ω (°)	132.35	132.42	132.38
K_1(km s^{-1})	242.72	244.63	246.77
K_2(km s^{-1})	247.68	241.42	244.69
K_1/K_2	0.9800	1.0133	1.0085

Notes. The anomalistic period, the rate of periastron advance, and eccentricity were kept fixed at values of $2^{\rm d}.996845$, 0.020645 degrees per day, and 0.1451. All epochs are in RJD.

4. Final elements

To derive the final solution leading to the improved values of the basic physical properties of the binary components and of the system, we had to proceed in an iterative way. One of us (JN) has developed a program that interpolates in the grid of synthetic spectra and by minimizing the difference between the observed and model spectra, estimates the optimal values of $T_{\rm eff}$, log g, $v \sin i$, and RV. The program was applied to disentangled spectra of both binary components using the NLTE line-blanketed spectra from the O-star grid published by Lanz & Hubeny (2003). We then used the resulting $T_{\rm eff}$ for star 1 and kept it fixed in the

Table 13. Final solution and absolute elements.

Element		Combined KOREL and PHOEBE solution Primary	System	Secondary
a	($R_\odot$)		28.72 fixed	
q			1.001 fixed	
$T_{\rm periastr.}$	(RJD)		46 308.66407 ± 0.00010	
$T_{\rm min.I}$	(RJD)		46 308.39658 ± 0.00010	
e			0.14508 fixed	
ω	(°)	132.514 ± 0.052		312.514
i	(°)		86.474 ± 0.019	
Ω		6.186 ± 0.014		6.162 ± 0.014
$T_{\rm eff}$	(K)	33200 ± 200 fixed		33521 ± 40
M	($M_\odot$)	17.72 ± 0.35		17.73 ± 0.30
R	($R_\odot$)	5.785 ± 0.091		5.816 ± 0.063
$M_{\rm bol}$	(mag)	−6.65 ± 0.04		−6.70 ± 0.04
log g	[cgs]	4.161 ± 0.014		4.157 ± 0.010
L_i	V band	0.496 ± 0.003		0.504
L_i	B band	0.496 ± 0.003		0.504
L_i	U band	0.495 ± 0.003		0.505
V_{1+2}	(mag.)		7.2845	
B_{1+2}	(mag.)		7.2296	
U_{1+2}	(mag.)		6.3137	
V_0	(mag.)	7.287		7.265
$(B-V)_0$	(mag.)	−0.291		−0.291
$(U-B)_0$	(mag.)	−1.086		−1.091
M_V	(mag.)	−3.59		−3.62

Notes. Ω is the value of the Roche-model potential used in the WD program, and L_i are the relative luminosities of the components in individual photometric passbands. They are normalised in such a way that $L_1 + L_2 = 1$.The system magnitudes at maximum light V_{1+2}, B_{1+2}, and U_{1+2} are based on the PHOEBE model light curves for the calibrated Hvar photometry.

light-curve solution in the program PHOEBE. This time, we used only the *UBV* observations that we transformed to the standard Johnson system i.e. the data from stations 1, 16, and 78 plus two good-quality sets of *BV* observations (stations 71 and 75) and the *R* photometry from station 2 in Table 3.

We note that KOREL also allows the determination of RVs of individual components. However, when these RVs are used in FOTEL, they lead to an orbital solution, which differs somewhat from that derived by KOREL. The reason is that the RVs are derived from individual spectra (of varying S/N), while the orbital elements in KOREL are given by the whole ensemble of the spectra, weighted by the square of their S/N (cf. Eq. (5)).

We therefore adopted the mean values from the three solutions in Table 12,

$$K_1 = 244.7 \pm 2.0 \text{ km s}^{-1}, \quad K_2 = 244.6 \pm 3.1 \text{ km s}^{-1},$$
$$q = 1.001 \pm 0.015,$$

to derive the semi-major axis $a = (28.72 \pm 0.22)\, R_\odot$. It was then, together with q, fixed in PHOEBE to reproduce the KOREL orbital solution.

For the eccentricity of 0.14508 one can estimate that the synchronization at periastron would require the angular rotational speeds of the binary components to be 1.354 times faster than the orbital angular speed. We fixed this value in PHOEBE. Using the radii of the components resulting from the PHOEBE solution, we estimate $v \sin i = 132$ km s^{-1} for both binary components.

When PHOEBE converged, we used the resulting log g and the relative luminosities L_1 and L_2 (expressed in units of the total luminosity outside eclipses) for both components and kept them fixed for another fit of disentangled spectra. A new value of $T_{\rm eff1}$ was then used in PHOEBE. We arrived at a final set of elements after three such iterative cycles. The final solution is presented in detail in Table 13 and the disentangled and model spectra are compared in Fig. 6.

The dereddened colours of the binary components correspond well to their spectral class O9.5 and the solution implies a distance modulus of 10.9, consistently for both binary components. The corresponding parallax of 0.″00066 does not contradict the HIPPARCOS revised parallax of 0.″00080 ± 0.″00046 (van Leeuwen 2007a,b).

5. A negative search for rapid line-profile variations

To check whether or not line profile variability (LPV) is present in either component of Y Cyg, we first used KOREL to generate difference spectra for each component. This was done once the solutions had been converged properly. Essentially, KOREL shifts a recovered component line profile to the appropriate radial velocity, and then subtracts the line profile from the observed spectrum. If any LPV is present, it should be easily detectable in these difference spectra. The temporal variance spectrum TVS (Fullerton et al. 1996) was used to search for any signature of LPV in the He I 4388 line. This line was chosen because there are no nearby strong blends. Upon investigating both TVS plots, we conclude that no LPV, detectable at the level of accuracy of our data, is present. If LPVs *were* present, one would see sharp peaks in the TVS rising above the noise level at the location of the line, which is not the case.

6. Conclusions

The results of a very detailed study of a huge body of spectral and photometric observations of an archetypal early-type

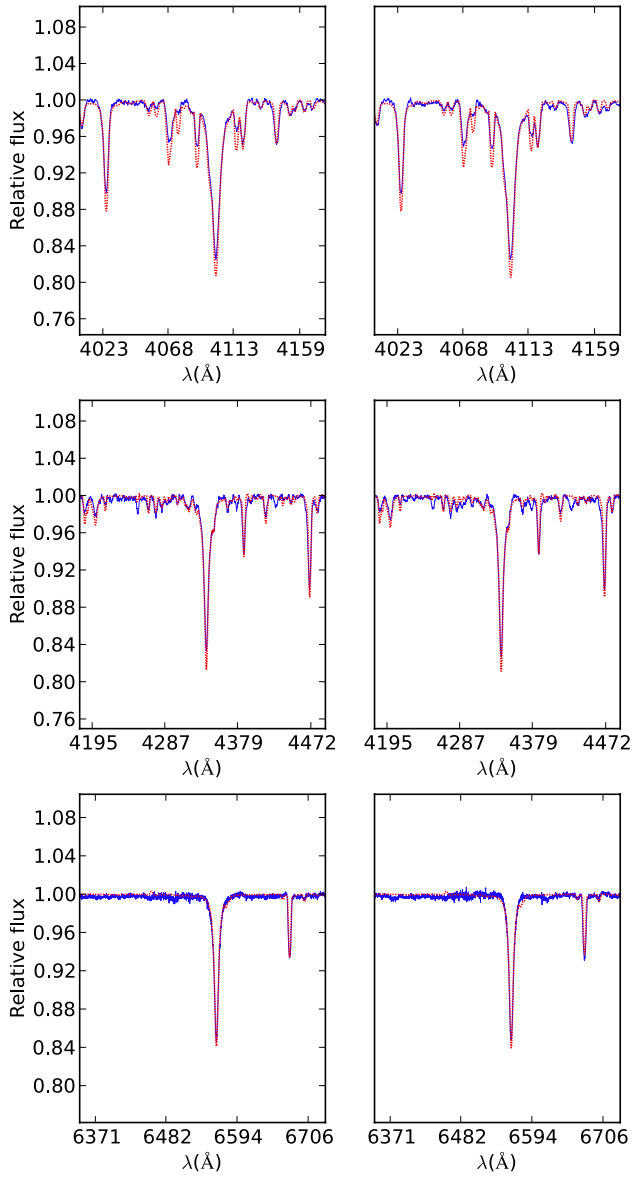

Fig. 6. Comparison of the KOREL disentangled spectra (solid/blue line) with synthetic spectra (dotted/red thin line). The *left panels* show the spectrum of the primary compared to the synthetic spectrum with $T_{\rm eff}$ = 33 200 K, log g = 4.161 [cgs], $v \sin i$ = 132 km s^{-1}, and a relative luminosity 0.496. The *right panels* show the spectrum of the secondary compared to the model spectrum with $T_{\rm eff}$ = 33 521 K, log g = 4.17 [cgs] broadened to $v \sin i$ = 132 km s^{-1}, and a relative luminosity 0.504.

eclipsing binary with a fast apsidal motion can be summarized as follows:

1. A comparison of separate analyses of radial-velocity and photometric observations and of recorded times of minima covering about 130 years shows that mutually consistent determinations of the sidereal and anomalistic period and the period of apsidal-line rotation are obtained. The most accurate results are based on the PHOEBE analysis of all complete light curves.
2. The new values of masses, radii, effective temperatures, and luminosities of the binary components are now quite robust and indicate a close similarity of both bodies. However, it is a bit disappointing that these new solutions do not represent a substantial improvement over the previously published determinations. The problem arises partly from the fact that all electronic spectra at our disposal have a moderate spectral resolution (from 13 000 to 20 000), and partly in inherent problems on the side of theory. For instance, we were unable to achieve a perfect match between the disentangled and synthetic spectra. In addition, the true uncertainties in the estimated effective temperatures are surely much higher than the formal errors in the final solution. We note that Hill & Holmgren (1995) estimated effective temperatures 31 000 ± 2000 K and 31 600 ± 2000 K and log g = 4.00 [cgs] and 4.00 [cgs] for stars 1 and 2, respectively. Simon et al. (1994) carried out a detailed comparison of the observed and synthetic NLTE spectra derived by Kunze (1990, 1994) and arrived at $T_{\rm eff1}$ = 34 200 ± 600 K, $T_{\rm eff2}$ = 34 500 ± 600 K, log g_1 = 4.18 [cgs], and log g_2 = 4.16 [cgs]. As pointed out to us by Hubeny (2013, priv. comm.), the theoretical spectra computed by Kunze do not include the metal line blanketing. This indicates that they probably *overestimate* the effective temperatures by as much as ~2000 K. Even when one compares the synthetic spectra from the O-star grid, and the later published spectra from the B-star grid (Lanz & Hubeny 2007) in the overlapping temperature range, it turns out that the two sets of model spectra differ from each other since the B-star values are based on somewhat improved input physics. Clearly, without further progress in the model spectra, one cannot do any better.
3. We also note that our new masses, radii, and effective temperatures, together with the observed rate of the apsidal motion, imply the relativistic contribution to the apsidal motion $\dot{\omega}_{\rm rel.}$ = 0.0009645 °d^{-1}, i.e. about 4.6% of the total observed rate of the apsidal rotation. This implies the observed value of the logarithm of the internal structure constant (average of the two nearly identical stars) log k_2 = −1.937 ± 0.011. In Fig. 7 we compare the range of this observed value (within the quoted error) with the evolutionary models of Claret (2004). The observed and theoretical values agree with each other for an evolutionary age slightly over 2 × 10^6 yr.

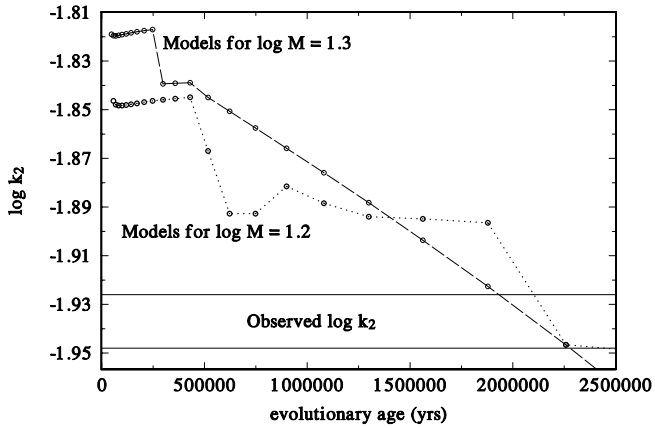

Fig. 7. Comparison of the observed range of the logarithm of the internal structure constant with its theoretical value based on the evolutionary models of Claret (2004), calculated for log M 1.2 and 1.3 (masses 15.85 $M_\odot$ and 19.95 $M_\odot$, respectively). The observed and theoretical values agree for an evolutionary age slightly over 2 000 000 years.

Acknowledgements. DH would like to thank the director and staff of the Dominion Astrophysical Observatory for the generous allocation of observing time and technical assistance. We thank Dr. L.V. Mossakovskaya who kindly provided us with her unpublished V observations of two minima secured in 1989 and 1990. Dr. Ž. Ivezić kindly helped us to obtain a copy of Dugan's paper with the visual photometry of Y Cyg. The use of the following internet-based resources is gratefully acknowledged: the SIMBAD database and the VizieR service operated at CDS, Strasbourg, France; the NASA's Astrophysics Data

System Bibliographic Services, and the O–C gateway of the Czech Astronomical Society[2]. In the initial stage, this study was supported by the grant A3003805 of the Grant Agency of the Academy of Sciences of the Czech Republic. Later, it was supported by the grants GA ČR 205/03/0788, 205/06/0304, 205/06/0584, and 209/10/0715 of the Czech Science Foundation and also by the research projects AV0Z10030501 and MSM0021620860. E.F. Guinan and G. McCook wish to acknowledge support from the US National Science Foundation Grants NSF/RUI AST-0507536 and AST-1009903.

References

Abt, H. A. 1973, ApJS, 26, 365
Al-Naimiy, H. M. 1978, Ap&SS, 53, 181
Burkholder, V., Massey, P., & Morrell, N. 1997, ApJ, 490, 328
Castelli, F., & Kurucz, R. L. 2004, Modeling of stellar atmosphers, IAU Symp., eds. N. Piskunor et al. [arXiv:astro-ph/0405087]
Claret, A. 2000, A&A, 363, 1081
Claret, A. 2004, A&A, 424, 919
Diaz-Cordoves, J., Claret, A., & Giménez, A. 1995, A&AS, 110, 329
Dugan, R. S. 1931, Contributions from the Princeton University Observatory, 12, 1
Fox, G. K. 1994, PASP, 106, 370
Fullerton, A. W., Gies, D. R., & Bolton, C. T. 1996, ApJS, 103, 475
Giménez, A., & Bastero, M. 1995, Ap&SS, 226, 99
Giménez, A., & Costa, V. 1980, PASP, 92, 782
Giménez, A., & García-Pelayo, J. M. 1983, Ap&SS, 92, 203
Giménez, A., Kim, C.-H., & Nha, I.-S. 1987, MNRAS, 224, 543
Hadrava, P. 1990, Contributions of the Astronomical Observatory Skalnaté Pleso, 20, 23
Hadrava, P. 1995, A&AS, 114, 393
Hadrava, P. 1997, A&AS, 122, 581
Hadrava, P. 2004a, Publ. Astron. Inst. Acad. Sci. Czech Rep., 92, 1
Hadrava, P. 2004b, Publ. Astron. Inst. Acad. Sci. Czech Rep., 92, 15
Hadrava, P. 2005, Ap&SS, 296, 239
Harmanec, P. 1998, A&A, 335, 173
Harmanec, P., Hadrava, P., Yang, S., et al. 1997, A&A, 319, 867
Herczeg, T. 1972, A&A, 20, 201
Hill, G. 1982, Publ. Dominion Astrophysical Observatory Victoria, 16, 67
Hill, G., & Holmgren, D. E. 1995, A&A, 297, 127
Holmgren, D., Hill, G., & Scarfe, C. D. 1995, The Observatory, 115, 188
Holmgren, D., Hadrava, P., Harmanec, P., Koubský, P., & Kubát, J. 1997, A&A, 322, 565
Horn, J., Kubát, J., Harmanec, P., et al. 1996, A&A, 309, 521
Huffer, R. C., & Karle, J. H. 1959, ApJ, 129, 237
Karami, K., & Teimoorinia, H. 2007, Ap&SS, 311, 435
Karami, K., Ghaderi, K., Mohebi, R., Sadeghi, R., & Soltanzadeh, M. M. 2009, Astron. Nachr., 330, 836
Koch, R. H., & Pfeiffer, R. J. 1989, PASP, 101, 279
Kunze, D. 1990, in Properties of Hot Luminous Stars, ed. C. D. Garmany, ASP Conf. Ser., 7, 90
Kunze, D. 1994, Ph.D. thesis, Ludwig-Maximilians Universität, Munich, Germany
Lanz, T., & Hubeny, I. 2003, ApJS, 146, 417
Lanz, T., & Hubeny, I. 2007, ApJS, 169, 83
Magalashvili, N. L., & Kumsishvili, J. I. 1959, Abastumanskaia Astrofizicheskaia Observatoriia Biulleten, 24, 13
Morrison, N. D., & Garmany, C. D. 1984, in NASA Conf. Publ. 2349, eds. J. M. Mead, R. D. Chapman, & Y. Kondo, 373
Mossakovskaya, L. V. 2003, Informational Bulletin on Variable Stars, 5393, 1
O'Connell, D. J. K. 1977, Ricerche Astronomiche, 8, 543
Perryman, M. A. C., & ESA 1997, The Hipparcos and Tycho catalogues, Astrometric and photometric star catalogues derived from the ESA Hipparcos Space Astrometry Mission (Noordwijk, Netherlands: ESA Publications Division), ESA SP Series 1200
Pfeiffer, R. J., Pachoulakis, I., Koch, R. H., & Stickland, D. J. 1994, The Observatory, 114, 297
Plaskett, J. S. 1920, Publications of the Dominion Astrophysical Observatory Victoria, 1, 213
Prša, A., & Zwitter, T. 2005, ApJ, 628, 426
Prša, A., & Zwitter, T. 2006, Ap&SS, 36
Redman, R. O. 1930, Publications of the Dominion Astrophysical Observatory Victoria, 4, 341
Richardson, E. H. 1968, JRASC, 62, 313
Simon, K. P., & Sturm, E. 1992, in Astronomische Gesellschaft Abstract Series, ed. G. Klare, 7, 190
Simon, K. P., & Sturm, E. 1994, A&A, 281, 286
Simon, K. P., Sturm, E., & Fiedler, A. 1994, A&A, 292, 507
Škoda, P. 1996, in Astronomical Data Analysis Software and Systems V, ASP Conf. Ser., 101, 187
Stickland, D. J., Lloyd, C., Koch, R. H., Pachoulakis, I., & Pfeiffer, R. J. 1992, The Observatory, 112, 150
Struve, O., Sahade, J., & Zebergs, V. 1959, ApJ, 129, 59
van Leeuwen, F. 2007a, in Astrophys. Space Sci. Lib., ed. F. van Leeuwen (Germany: Springer), 350
van Leeuwen, F. 2007b, A&A, 474, 653
Vitrichenko, E. A. 1971, Izv. Krymskoj Astrofizicheskoj Observatorii, 43, 71
Wade, R. A., & Rucinski, S. M. 1985, A&AS, 60, 471
Wilson, R. E., & Devinney, E. J. 1971, ApJ, 166, 605
Wolf, M., Harmanec, P., Holmgren, D. E., et al. 2013, in Massive Stars: From alpha to Omega, Poster at the Conf. Rhodes, Greece, id. 107, http://a2omega-conference.net

[2] http://var.astro.cz/ocgate/

Appendix A: Details of the reduction and transformation of photometric data

Comments on individual data sets:

Station 19: Abastumani 0.48 m reflector

These observations are on an instrumental *UBV* system and suffer from an unusually large scatter. Moreover, the last night (HJD 2 441 154) seems to deviate from the general light curve quite a lot. In addition, the times of the inflection inside the light minimum differ notably for different passbands for this particular night. Since we now have at our disposal numerous observations covering a similar period of time, we excluded these definitely lower-quality data from our analyses.

Station 42: *Dyer*

A very limited set of instrumental *UBV* observations from three nights only.

Station 70: *Mojon de Trigo*

The data for the night HJD 2 444 083 in Table I of Giménez & Costa (1980) are not presented in an increasing order which looks a bit confusing, but there is no actual misprint in the table, as kindly communicated to us by Dr. Alvaro Giménez. The data are on an instrumental system.

Station 71: *Vatican*

According to O'Connell (1977), these data were transformed to the standard Johnson system using observations of several *UBV* standards. In addition, the extinction was derived and appropriate corrections were applied. We note that there is an obvious misprint in the first observation, obtained on HJD 2 439 712.3492, at the *U* colour: It should read –0$^{\rm m}$.641 instead of the tabulated value of –0$^{\rm m}$.941.

Station 72: *University of Victoria 0.30 m*

These are data on an instrumental *UBV* system. No extinction corrections were applied.

Station 74: *Abastumani 0.33 m*

This is the largest homogeneous set of photoelectric observations of Y Cyg, covering the period from 1950 to 1957. The data were obtained without any filter and the check star used, HD 197 419, is listed under the name V568 Cyg in the General Catalogue of Variable Stars. There is a misprint in the last page of Table 1 of Magalashvili & Kumsishvili (1959): the first Julian date is HJD 2 435 663 (continuation from the previous page), not 2 435 659 as given in the Table. The data are of a good quality, with the exception of the following deviating observations which we omitted from our analysis: HJD 2 434 209.316, all three observations from 2434897, 2 434 949.298, 2 435 635.408, .423, 2 435 647.365, 2 436 071.339, and .342.

Station 75: *Tübingen 0.40 m*

A limited set of instrumental *BV* observations.

Station 76: *Hoher List*

These early blue and yellow observations are on an instrumental system. They were secured relative to a red comparison star HD 198 692.

Station 77: *IUE Fine Error Sensor*

These observations, transformed to Johnson *V* by Stickland et al. (1992), come from two tracking stations. They have larger scatter than most of the photoelectric observations secured on the Earth, but their time distribution ensures a relatively uniform, although not dense coverage of the light curve. There is one deviating point at HJD 2 448 040.442 that we omitted from the analyses.

Table A.1. Standard *UBV* magnitudes of all comparison stars used by various investigators in their differential photometries of Y Cyg.

Star	HD	V	$(B-V)$	$(U-B)$	No.	Station
BD+33°4062	–	$9^{\rm m}.402 \pm 0.011$	$0^{\rm m}.487$	$0^{\rm m}.018$	9	01
BD+34°4180	198 692	$6^{\rm m}.647 \pm 0.011$	$1^{\rm m}.018$	$0^{\rm m}.802$	33	01
BD+34°4180	198 692	$6^{\rm m}.637 \pm 0.007$	$1^{\rm m}.027$	$0^{\rm m}.832$	11	16
BD+34°4180	198 692	$6^{\rm m}.645 \pm 0.008$	–	–	146	61
BD+34°4180	198 692	$6^{\rm m}.633 \pm 0.011$	$1^{\rm m}.029$	$0^{\rm m}.811$	56	78
HR 7996	198 820	$6^{\rm m}.421 \pm 0.007$	$-0^{\rm m}.132$	$-0^{\rm m}.618$	8	01
HR 7996	198 820	$6^{\rm m}.424 \pm 0.007$	–	–	214	61
BD+34°4196	199 007	$7^{\rm m}.953 \pm 0.014$	$-0^{\rm m}.059$	$-0^{\rm m}.310$	72	01
BD+34°4196	199 007	$7^{\rm m}.950 \pm 0.007$	$-0^{\rm m}.059$	$-0^{\rm m}.319$	11	16
BD+34°4196	199 007	$7^{\rm m}.959 \pm 0.012$	–	–	138	61
BD+34°4196	199 007	$7^{\rm m}.955 \pm 0.014$	$-0^{\rm m}.060$	$-0^{\rm m}.310$	99	78
BD+37°4235	202 349	$7^{\rm m}.354 \pm 0.009$	$-0^{\rm m}.167$	$-0^{\rm m}.971$	149	01
BD+37°4235	202 349	$7^{\rm m}.356 \pm 0.010$			161	61
70 Cyg	204 403	$5^{\rm m}.307 \pm 0.009$	$-0^{\rm m}.149$	$-0^{\rm m}.654$	108	01
70 Cyg	204 403	$5^{\rm m}.306 \pm 0.007$	$-0^{\rm m}.149$	$-0^{\rm m}.655$	58	16
70 Cyg	204 403	$5^{\rm m}.307 \pm 0.006$	–	–	200	61
70 Cyg	204 403	$5^{\rm m}.307 \pm 0.012$	$-0^{\rm m}.149$	$-0^{\rm m}.655$	109	78

Notes. The values we derived from the calibrated and carefully reduced all-sky *UBV* observations obtained during several seasons at Hvar (station 01) were added to the appropriate magnitude differences for all differential data sets from the literature. We also tabulate the mean all-sky values derived from the final reduction of Fairborn APT and Sejong observations. For comparison, the mean *V* magnitude based on the transformation of the HIPPARCOS H_p magnitude to Johnson *V* after Harmanec (1998) is also tabulated for all comparison stars used. The number (No.) of individual calibrated all-sky observations on which the mean values are based is also given. Stations: 1) Hvar; 16) Fairborn T5; 61) HIPPARCOS; 78) Sejong.